

Basic Neuroscience

The effects of lobeline on $\alpha 4\beta 2^*$ nicotinic acetylcholine receptor binding and uptake of [^{18}F]nifene in ratsAnsel T. Hillmer^{a,b,*}, Dustin W. Wooten^{a,b}, Mohammed Farhoud^c, Todd E. Barnhart^a, Jogeshwar Mukherjee^d, Bradley T. Christian^{a,b,e}^a Department of Medical Physics, University of Wisconsin–Madison, 1111 Highland Avenue, Room 1005, Madison, WI 53705, United States^b Waisman Brain Imaging Laboratory, University of Wisconsin–Madison, 1500 Highland Avenue, Madison, WI 53705, United States^c Comprehensive Cancer Center, University of Wisconsin–Madison, 1111 Highland Avenue, Room 7057, Madison, WI 53705, United States^d Department of Radiological Sciences, University of California–Irvine, B140 Medical Sciences, Irvine, CA 92697, United States^e Department of Psychiatry, University of Wisconsin–Madison, 6001 Research Park Blvd, Madison, WI 53719, United States

HIGHLIGHTS

- ▶ Lobeline interacts with $\alpha 4\beta 2^*$ nAChRs and the BBB amine transporter.
- ▶ PET imaging in rats assessed the interaction of lobeline with [^{18}F]nifene *in vivo*.
- ▶ Lobeline competes strongly with [^{18}F]nifene at the $\alpha 4\beta 2^*$ site.
- ▶ The cerebellum is not a valid reference region for [^{18}F]nifene in the rat.
- ▶ Small decreases in [^{18}F]nifene BBB transport rates were observed due to lobeline.

ARTICLE INFO

Article history:

Received 28 November 2012

Received in revised form 15 January 2013

Accepted 18 January 2013

Keywords:

[^{18}F]nifene

Nicotinic acetylcholine receptor

PET

lobeline

BBB amine transporter

Smoking cessation

ABSTRACT

Lobeline is a potential smoking cessation drug with affinity for the $\alpha 4\beta 2$ nicotinic acetylcholine receptor and may inhibit the blood–brain barrier (BBB) amine transporter. The goal of this work was to use PET imaging to evaluate the effects of lobeline on the kinetic properties of [^{18}F]nifene in the rat brain. **Methods:** Direct $\alpha 4\beta 2^*$ competition of lobeline with [^{18}F]nifene was evaluated using imaging experiments with both displacing and blocking doses of lobeline (1 mg/kg, i.v.) given between two injections of [^{18}F]nifene separated by 50 min. Inhibition of the BBB amine transporter was examined using a separate imaging protocol with three injections of [^{18}F]nifene, first at baseline, then following (–)nicotine blocking, and finally following lobeline blocking. **Results:** Rapid displacement of [^{18}F]nifene was observed in the $\alpha 4\beta 2^*$ -rich thalamus following lobeline administration, suggesting direct competition of the drug at $\alpha 4\beta 2^*$ sites. Slight decreases in BBB transport of [^{18}F]nifene were observed when the $\alpha 4\beta 2^*$ system was first saturated with (–)nicotine and then given lobeline. This perturbation may be due to inhibition of the BBB amine transporter by lobeline or reductions in blood flow. Significant cerebellar displacement of [^{18}F]nifene was found following the administration of both lobeline and (–)nicotine, indicating detectable specific binding in the rat cerebellum. **Conclusion:** The competition of lobeline with [^{18}F]nifene is largely dominated at the $\alpha 4\beta 2^*$ binding site and only small perturbations in BBB transport of [^{18}F]nifene are seen at the 1 mg/kg dose. Similar experiments could be used to study other drugs as therapeutic agents for smoking cessation with PET.

© 2013 Elsevier B.V. All rights reserved.

Abbreviations: BBB, blood–brain barrier; B/F, bound-to-free ratio; nAChR, nicotinic acetylcholine receptor; PET, positron emission tomography; 1TCM, one tissue compartment model.

* Corresponding author at: Department of Medical Physics, University of Wisconsin–Madison, 1111 Highland Avenue, Madison, WI 53705, United States. Tel.: +1 608 890 2959; fax: +1 608 890 1897.

E-mail addresses: ahillmer@wisc.edu (A.T. Hillmer), dwooten@wisc.edu (D.W. Wooten), mfarhoud@wisc.edu (M. Farhoud), tebarnhart@wisc.edu (T.E. Barnhart), mukherj@uci.edu (J. Mukherjee), bchristian@wisc.edu (B.T. Christian).

1. Introduction

The $\alpha 4\beta 2$ nicotinic acetylcholine receptor (nAChR) system is an important target for understanding the basis of a wide variety of neuropathologies. NACHRs have been implicated in Alzheimer's disease (Court et al., 2001), Parkinson's disease (Burghaus et al., 2003), and tobacco addiction (Poirier et al., 2002), as well as other neurodevelopmental and neurodegenerative processes (Albuquerque et al., 2009). The agonist radioligand, [^{18}F]nifene, was developed as a marker for $\alpha 4\beta 2^*$ nAChRs (the * denotes low levels of binding to other subtypes with $\alpha 4$ or $\beta 2$ subunits) with

positron emission tomography (PET) imaging (Pichika et al., 2006). Our earlier work found high uptake of [^{18}F]nifene consistent with $\alpha 4\beta 2$ nAChR distribution in the rhesus monkey brain (Hillmer et al., 2011). [^{18}F]Nifene also exhibits fast kinetic properties resulting in accurate quantification of binding potentials in scan times of 45 min, demonstrating utility for investigating processes involving $\alpha 4\beta 2^*$ nAChRs (Hillmer et al., 2012).

Recent experiments with [^{18}F]nifene in the rat found similar binding distributions and kinetic properties, however, evaluation of the cerebellum as a suitable reference region was inconclusive (Kant et al., 2011). The determination of a suitable reference region is a critical validation step for analysis of binding levels in single injection PET studies. Since the cerebellum is a large structure easily delineated without auxiliary MRI data and often contains low receptor levels for neurotransmitters of interest (i.e. dopamine, serotonin), it is commonly evaluated as such a reference region. Previous *in vitro* studies have shown the cerebellum to contain low levels of $\alpha 4\beta 2^*$ nAChRs (Happe et al., 1994), making it a candidate reference region for evaluation.

The primary mechanism of action for the drug lobeline occurs at the $\alpha 4\beta 2^*$ nAChR site where lobeline binds with nanomolar affinity (Brioni et al., 1996). Interestingly, lobeline has been found to antagonize the effects of nicotine without eliciting a neural response from nAChRs. Therefore, lobeline has been considered as a potential treatment for smoking cessation (Damaj et al., 1997). Previous studies have also demonstrated that lobeline blocks the blood–brain barrier (BBB) basic amine transporter with a sub-millimolar inhibition constant (Allen et al., 2003). In addition to nAChRs, lobeline has affinity for μ -opioid receptors at sub-micromolar affinities (Miller et al., 2007), and roughly 1–100 μmol affinities for a wide variety of monoamine transporters, including VMAT2, DAT, SERT, and NET (Miller et al., 2004; Teng et al., 1997). The chemical structures of lobeline, [^{18}F]nifene, and nicotine are shown in Fig. 1. The high affinity of lobeline for the $\alpha 4\beta 2$ nAChR and its inhibition of the BBB amine transporter make it an appealing compound for use in studying the *in vivo* kinetics of $\alpha 4\beta 2^*$ nAChR radioligands with PET imaging.

The main aim of this work was to use dynamic PET imaging in the rat brain to assess competition between lobeline and [^{18}F]nifene at both the $\alpha 4\beta 2^*$ nAChR site and the BBB amine transporter. The effects of lobeline on the *in vivo* kinetics of [^{18}F]nifene were therefore examined in these two contexts. An ancillary goal was to determine the extent of [^{18}F]nifene binding in the rat cerebellum to evaluate the use of this region as a reference. Knowledge of the mechanisms of lobeline competition with [^{18}F]nifene will provide valuable information for the development of PET experiments to study the $\alpha 4\beta 2^*$ nAChR system. These imaging experiments also represent alternative methods for interrogating the effects of smoking cessation therapeutics such as lobeline on the nicotinic acetylcholine neurotransmitter system.

2. Materials and methods

2.1. Subjects and materials

The radiosynthesis of 2-[^{18}F]fluoro-3-[2-((S)-3-pyrrolinyl)methoxy]pyridine ([^{18}F]nifene) was performed according to previously reported methods (Hillmer et al., 2012). Specific activities were in excess of 150 GBq/ μmol at the time of scan start. The nitro precursor was obtained from ABX (Radeberg, Germany). (–)Nicotine hydrogen tartrate salt was purchased from Sigma–Aldrich (St. Louis, MO). Lobeline hydrochloride was acquired from TCI America (Portland, OR). Two female Sprague–Dawley rats (170 g, 190 g) were acquired from Charles River Laboratories, Inc. (Wilmington, MA). All housing and experimental

protocols were approved by the institutional animal care and use committee (IACUC).

2.2. PET procedures

For all PET experiments, subjects were initially anesthetized with 5.0% isoflurane, then maintained with 2–3% isoflurane administered via a nose cone for the duration of the PET experiments. The subjects were placed on a heating pad, with heart and respiration rates monitored throughout the experiment (BioVet Suite with heating pad upgrade, M2M Imaging). Subjects were positioned with the brain at the isocenter of the PET scanner. PET data were acquired with a Siemens microPET Inveon scanner, which has a field of view of 12.7 cm in the axial direction and 10 cm in the transaxial direction with a reported in-plane spatial resolution of 1.5 mm (Constantinescu and Mukherjee, 2009). After acquiring the emission data, the bed was removed from the microPET scanner and transferred to the adjacent microCT Inveon scanner to acquire X-ray transmission data for scatter and attenuation correction. Following completion of the transmission scan the subject was returned to its cage and monitored until fully alert.

Two different PET scanning protocols, each described in detail below, were used for the present work. A visual schematic of both protocols is illustrated in Fig. 2. Each protocol was conducted twice, once on each of two rat subjects. At least two weeks passed between each experiment to prevent residual drug from interfering with future studies.

In the first experimental protocol, conducted with each of the two subjects, an i.v. injection of approximately 30 MBq high specific activity [^{18}F]nifene in 500 μL saline was given simultaneously with the initiation of data acquisition. PET data was continuously acquired throughout the experiment for a total of 90 min. After 40 min of data acquisition, 1.0 mg/kg lobeline hydrochloride in 300 μL saline was administered intravenously to examine competitive binding with [^{18}F]nifene. A second lobeline dose (1.0 mg/kg in 300 μL saline) was administered 49 min after scan start to ensure complete $\alpha 4\beta 2^*$ saturation by lobeline. After 50 min of data acquisition (1 min after the second lobeline dose), an injection of 22–30 MBq [^{18}F]nifene was given to examine changes in cerebellar kinetics before and after lobeline.

A second experiment was designed to first fully saturate the $\alpha 4\beta 2^*$ system with (–)nicotine to isolate the BBB transport process for subsequent injections of [^{18}F]nifene. Acquisition of PET data began with the intravenous administration of approximately 45 MBq high specific activity [^{18}F]nifene in 300 μL saline. After 30 min of data acquisition, 0.92 mg/kg (–)nicotine hydrogen tartrate salt (0.3 mg/kg free base) in 300 μL saline (i.v.) was administered to displace specifically bound [^{18}F]nifene. A second injection of 30–35 MBq [^{18}F]nifene was administered 40 min after scan start to track radioligand kinetics under $\alpha 4\beta 2^*$ saturation conditions. After 63 min of data acquisition, lobeline (1.0 mg/kg in 300 μL saline, i.v.) was administered. A third [^{18}F]nifene injection of 33–37 MBq was given two minutes after the lobeline, 65 min into PET data acquisition, to examine changes in [^{18}F]nifene plasma-to-tissue transport and efflux in the presence of lobeline. The total duration of PET acquisition for the second experiment was 90 min.

2.3. PET image analysis

The PET time series were binned from list mode data into time frames ranging from 30 s to 120 s. Data reconstruction was performed using filtered back projection with a 0.5 cm^{-1} ramp filter, and included corrections for arc, scatter, attenuation, and scanner normalization. The resulting images were denoised with the HYPR-LR algorithm (Christian et al., 2010) using a $3 \times 3 \times 4$ voxel kernel. The final images contained a

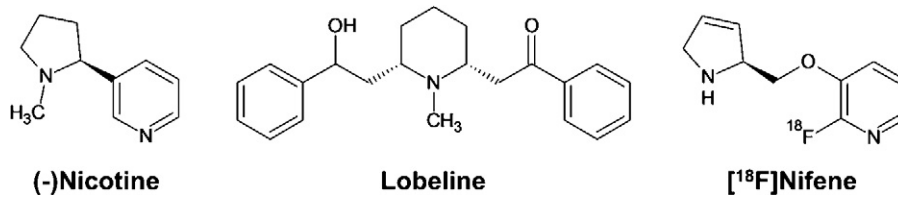


Fig. 1. $\alpha 4\beta 2$ nAChR ligands. Chemical structures of compounds with high affinity for the $\alpha 4\beta 2$ nAChR site: (-)-nicotine, lobeline, and [¹⁸F]nifene.

matrix size of $128 \times 128 \times 159$ corresponding to voxel dimensions of $0.78 \text{ mm} \times 0.78 \text{ mm} \times 0.90 \text{ mm}$. No decay correction was performed on the data.

Regions of interest were hand drawn with multiple circles on late summed images using a rat brain atlas to guide region selection (Paxinos and Watson, 1998). The thalamus was selected as a region with high $\alpha 4\beta 2^*$ nAChR concentration. The cerebellum was chosen as a region with low $\alpha 4\beta 2^*$ nAChR expression (Happe et al., 1994) and [¹⁸F]nifene uptake levels (Kant et al., 2011). The resulting thalamic region had a volume of 35 mm^3 and the cerebellum region had a volume of 28 mm^3 .

To assess specific binding levels and directly compare radioligand uptake rates from different [¹⁸F]nifene injections, it was necessary to separately identify the contribution of each injection to the total observed PET signal. To accomplish this, the residual activity from each injection had to be subtracted from all subsequent injections. The design of both experimental protocols presented herein included the presence of drugs competing with [¹⁸F]nifene at the $\alpha 4\beta 2^*$ nAChR site prior to the second and third [¹⁸F]nifene injections. Therefore, negligible specific binding was assumed before and during the second and third [¹⁸F]nifene injections for analysis. The time course of nondisplaceable [¹⁸F]nifene, which includes both free and nonspecifically bound radioligand, was parameterized with data from the second [¹⁸F]nifene injection to uniquely identify the contribution of each [¹⁸F]nifene injection to the observed PET signal.

Several assumptions were made to parameterize the time course of nondisplaceable [¹⁸F]nifene. First, the washout of nondisplaceable radioligand (C_{NDi}) for injection i was assumed to be of the simple exponential form $C_{NDi} = M_i e^{-\alpha t}$ for late times ($>15 \text{ min}$ postinjection) following the administration of radioligand. Second, the washout rate of nondisplaceable radioligand, α , was assumed constant throughout each experiment. Finally, the constant M_i was assumed proportional to the administered [¹⁸F]nifene radioactivity for each injection, such that $M_i = A \cdot D_i$, where D_i is the injected [¹⁸F]nifene radioactivity for the i th injection and A is a constant.

Since specific binding was present during the first injection, the time course of nondisplaceable radioligand was parameterized with data from the second injection as described below. In the absence of specific binding during the second injection, the measured PET signal, PET_2 , can be taken to be the sum of

nondisplaceable radioligand from the first and second injection, or $PET_2 = C_{ND1} + C_{ND2}$. Using the three assumptions described above, this relation can be expanded as $PET_2 = A \cdot D_1 e^{-\alpha t} + A \cdot D_2 e^{-\alpha(t-t_2)}$ where t_i is the time of radioligand administration for the i th injection. This equation can be simplified to $PET_2 = A(D_1 + D_2 e^{\alpha t_2}) e^{-\alpha t}$ which allows the data to be fit to a single decaying exponential function.

The cerebellar data from the second [¹⁸F]nifene injection was fit to the function $PET_2 = M_2 e^{-\alpha t}$ from 15 min postinjection until subsequent drug administration. This fit yielded the parameters M_2 and α . To describe C_{ND1} in the form $C_{ND1} = M_1 e^{-\alpha t}$, M_1 was derived with the relationship $M_1 = M_2 \cdot D_1 / (D_1 + D_2 e^{\alpha t_2})$. Once C_{ND1} and PET_2 were parameterized, C_{ND2} was determined by $C_{ND2} = PET_2 - C_{ND1}$ to yield the time course of nondisplaceable signal due exclusively to the second injection. Similarly, the third [¹⁸F]nifene injection C_{ND3} was determined with the relationship $C_{ND3} = PET_3 - C_{ND1}$.

Because no blood sampling was performed during these experiments, specific binding levels during the first high specific activity [¹⁸F]nifene injection were estimated with the ratio of bound radioligand to “free” radioligand, B/F (where free radioligand includes nonspecifically bound radioligand). This metric was measured with the relationship $B/F = (C_T - C_{ND1}) / C_{ND1}$ where C_T is the total radioligand concentration and C_{ND1} is the concentration of nondisplaceable (free and nonspecifically bound) radioligand during the first injection. Both C_T and C_{ND1} were estimated by averaging over 24–30 min after scan start. The B/F ratios were used to approximate [¹⁸F]nifene specific binding in both the thalamus and cerebellum.

2.4. Modeling simulations

Simulations were performed to reproduce the observed changes in radioligand transfer between the arterial plasma and tissue due to lobeline when the $\alpha 4\beta 2^*$ nAChRs were saturated. The one tissue compartment model (1TCM) was used to model the PET signal in the absence of specific binding. The state equation describing the 1TCM is: $dC_T/dt = K_1 C_A - k_2 C_T$ where C_T is the total concentration of radiotracer present in the tissue including free, specifically bound, and nonspecifically bound states (i.e. $C_T = C_{ND} + C_B$), and C_A is the concentration of parent radioligand in the arterial plasma. The rate constants K_1 and k_2 describe bidirectional transport of radioligand between the arterial plasma and the tissue. The PET signal is

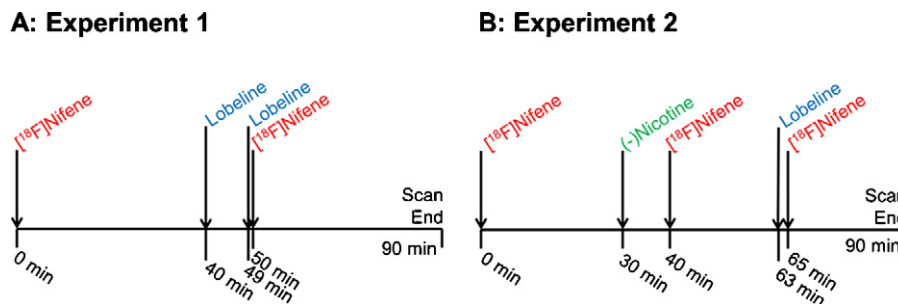


Fig. 2. Experimental designs. (A) Protocol of Experiment 1, designed to examine the effects of lobeline on [¹⁸F]nifene binding and uptake. (B) Protocol of Experiment 2, which eliminated specific [¹⁸F]nifene binding with (-)-nicotine to examine changes in [¹⁸F]nifene uptake rates due to lobeline.

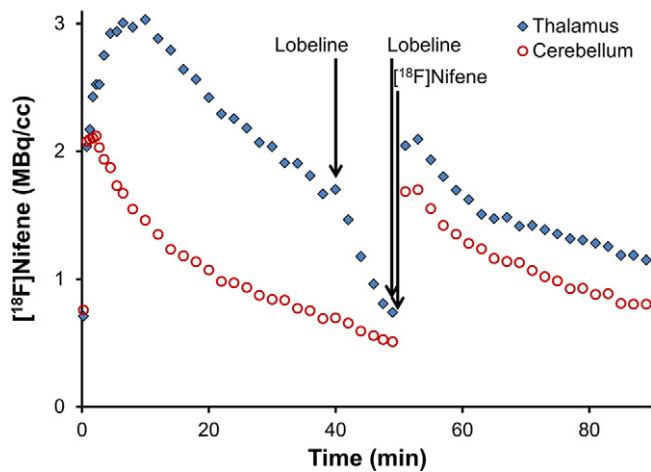


Fig. 3. Measured PET data from lobeline pre-blocking study, animal 1. The time course of two $[^{18}\text{F}]$ nifene injections separated by displacement and blocking injections of lobeline is shown. No corrections have been applied for injected activity or the decay of radioactivity.

modeled by $\text{PET} = C_T + f_v \cdot C_{WB}$ where the fractional blood volume f_v is assumed as $f_v = 0.04$, and C_{WB} is the concentration of radioactivity present in the whole blood. Simulations were performed with the COMKAT software (Muzic and Cornelius, 2001).

Simulated data sets were generated based on the arterial input function and rate constants found in our previous $[^{18}\text{F}]$ nifene studies with the rhesus monkey model (Hillmer et al., 2012). The 1TCM was used to first generate PET data approximating the observed PET signal due to nondisplaceable radioligand before the administration of lobeline with the rate constants $K_1 = 0.9 \text{ mL/min/mL}$ and $k_2 = 0.2 \text{ 1/min}$. This control simulation was then modified in two ways to qualitatively compare the perturbations in radioligand uptake rates in the presence of lobeline. First, the rate constants K_1 and k_2 were modified to simulate changes to the kinetic processes of $[^{18}\text{F}]$ nifene at the BBB. Second, the analytically defined input function was altered to mimic changes in the behavior of $[^{18}\text{F}]$ nifene in the plasma. A family of curves based on the original input function was generated where the area under the curve was preserved while the peak concentration and sharpness varied. The different input functions were then used to generate modeled PET signals using the same original rate constants. Therefore, alterations in the kinetic behavior of $[^{18}\text{F}]$ nifene in both the tissue and plasma due to lobeline were approximated with simulations.

3. Results

3.1. PET experiments

The first set of experiments administered lobeline to examine its effects on the displacement of bound $[^{18}\text{F}]$ nifene and subsequent blocking following a second $[^{18}\text{F}]$ nifene injection. Displacement of bound $[^{18}\text{F}]$ nifene was evident in the thalamus as shown in Fig. 3, with radioligand concentrations approaching cerebellar concentrations 10 min after the administration of lobeline. Slight displacement of bound $[^{18}\text{F}]$ nifene was also observed in the cerebellum, as the post-blocking injection of $[^{18}\text{F}]$ nifene revealed reduced radioligand binding when compared to the baseline data. Assuming complete cerebellar displacement of $[^{18}\text{F}]$ nifene by lobeline, B/F ratios of 0.2 and 0.2 in the cerebellum and 1.4 and 1.6 in the thalamus were observed for the two subjects, respectively.

Because perturbations to the $[^{18}\text{F}]$ nifene curves occurred in the cerebellum during the first set of experiments, it was not possible to distinguish lobeline's action at the $\alpha 4\beta 2^*$ receptor site from

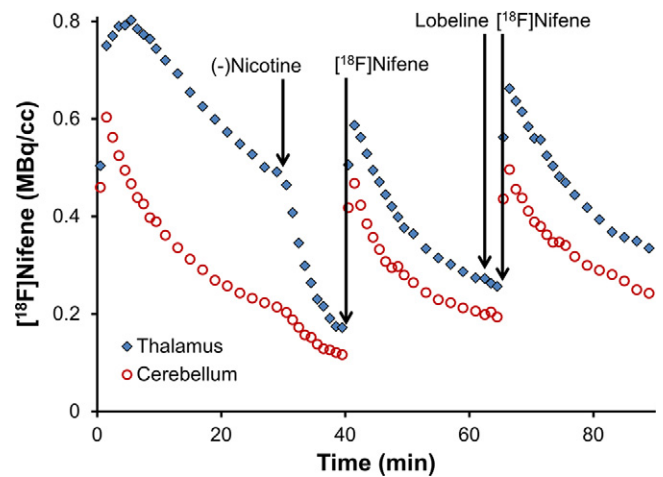


Fig. 4. Measured PET data from study with $(-)$ nicotine blocking followed by lobeline, animal 1. The time course of three $[^{18}\text{F}]$ nifene injections is shown. $(-)$ Nicotine was administered after the first injection to eliminate specific binding. The second $[^{18}\text{F}]$ nifene injection yields information on uptake rates of nifene in the absence of specific binding. The third $[^{18}\text{F}]$ nifene injection measures changes to uptake rates due to the presence of lobeline. No corrections have been applied for injected activity or the decay of radioactivity.

changes to plasma-to-tissue transport. Therefore, the main goal of the second set of experiments was to remove specific $\alpha 4\beta 2^*$ binding via blocking with $(-)$ nicotine to isolate the BBB transport of $[^{18}\text{F}]$ nifene and the effects of lobeline on this mechanism. Blocking of $[^{18}\text{F}]$ nifene binding in both the thalamus and cerebellum was observed, as shown in Fig. 4. The administration of $(-)$ nicotine elicited B/F ratios of 0.3 and 0.4 in the cerebellum and 2.4 and 2.2 in the thalamus for the two subjects, respectively.

The time courses of nondisplaceable radioligand from the first two $[^{18}\text{F}]$ nifene injections (C_{ND1} , C_{ND2}) were parameterized and subtracted from subsequent injections, as detailed in the methods and illustrated in Fig. 5A. The resulting concentrations of nondisplaceable $[^{18}\text{F}]$ nifene without lobeline (C_{ND2}) and with lobeline (C_{ND3}) were normalized to the $[^{18}\text{F}]$ nifene radioactivity administered for each injection and plotted on the same time scale to directly compare changes in uptake rates induced by lobeline, shown in Fig. 5B and C. The residual subtracted curves of $[^{18}\text{F}]$ nifene indicated that uptake in the cerebellum occurred more slowly in the presence of lobeline. Both time-activity curves from the second and third injections (C_{ND2} and C_{ND3} , respectively) followed roughly the same trajectory at later times post-injection. Heart rate and respiration rate were monitored throughout the duration of the experiments with no significant change to either measure throughout the course of the experiment.

3.2. Modeling simulations

Simulations were performed using the 1TCM (Fig. 6A) to replicate the changes in $[^{18}\text{F}]$ nifene uptake induced by lobeline observed in the second set of experiments (Fig. 5B–C). Simulations first focused on altering the transport parameters and found that reductions of 13% in both K_1 and k_2 , while holding their ratio constant, qualitatively resulted in similar changes in $[^{18}\text{F}]$ nifene uptake as illustrated in Fig. 6B. Additional simulations were then performed to examine the effects of blood flow changes on the shape of the arterial input functions while keeping the delivery time and area under the curve constant as shown in Fig. 6C. The resulting modeled PET signals (shown in Fig. 6D) revealed small changes in the modeled time-activity curve at early time points, whereas the later time points were similar for all input functions.

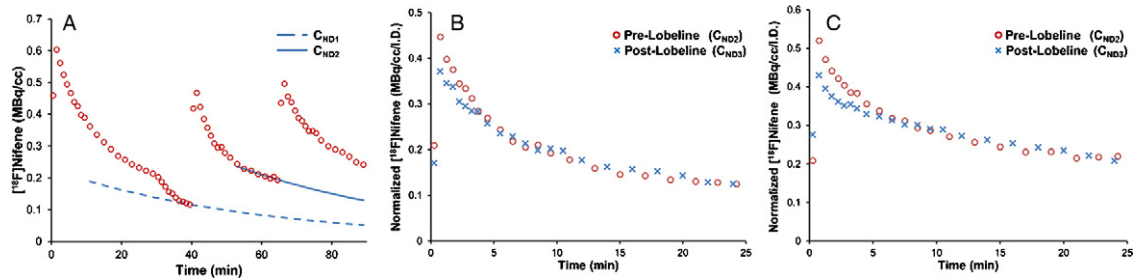


Fig. 5. Effects of lobeline on [^{18}F]nifene uptake rates in the cerebellum. (A) An illustration of the extrapolation fitting procedure used to derive curves of nondisplaceable uptake $C_{\text{ND}1}$ and $C_{\text{ND}2}$. The data is from animal 1. No corrections have been applied for injected activity or the decay of radioactivity. (B and C) A time-shifted overlay of the background subtracted time courses of [^{18}F]nifene before ($C_{\text{ND}2}$, \circ) and after ($C_{\text{ND}3}$, \times) the administration of lobeline for the two subjects (animals 1 and 2, respectively). These data (B and C) are scaled to the injected [^{18}F]nifene dose for each injection. The injection times are shifted to provide a direct comparison of the data following [^{18}F]nifene injections.

4. Discussion

Lobeline has two main mechanisms of action pharmacologically pertinent to the $\alpha 4\beta 2$ nAChR system, namely, high nanomolar affinity for the $\alpha 4\beta 2^*$ nAChR site comparable to that of (–)nicotine (Brioni et al., 1996), and inhibition of the BBB amine transporter (Allen et al., 2003). The effects of lobeline on [^{18}F]nifene kinetics in the rat model were investigated with the use of two experimental designs. The first experiment used lobeline to displace [^{18}F]nifene bound at the $\alpha 4\beta 2^*$ nAChR site. The second, more complex, experiment first saturated the $\alpha 4\beta 2^*$ nAChRs with (–)nicotine to isolate the kinetic effects of lobeline on transport of [^{18}F]nifene from the plasma to the tissue.

4.1. The effects of lobeline on [^{18}F]nifene binding

In the first experiments, lobeline (1 mg/kg i.v.) significantly displaced bound [^{18}F]nifene (see Fig. 3). Previous studies have found that a pre-blocking dose of 10–20 mg/kg lobeline administered subcutaneously lowered binding levels of $\alpha 4\beta 2^*$ nAChR PET radioligands (Horti et al., 1997; Kassiou et al., 1998), although this reduction was not as strong as those elicited by (–)nicotine or

cytisine. The present studies similarly found that cerebellar displacement of [^{18}F]nifene with lobeline was small compared to the effects of (–)nicotine (compare Figs. 3 and 4). Consequently, the B/F ratios were lower when nondisplaceable uptake was based on blockade of $\alpha 4\beta 2^*$ receptors with lobeline compared to nicotine. Since the administered 0.3 mg/kg (–)nicotine dose was previously found to displace 95% of bound [^{18}F]nifene (Kant et al., 2011), lobeline may incompletely displace bound radioligand at the given 1.0 mg/kg dosage.

The similarity of B/F ratios presented herein with those found by Kant et al. (2011) and our previous studies in rhesus monkeys (Hillmer et al., 2012) suggest that no residual mass effects occurred from the first [^{18}F]nifene injection. Based on our previous measurement of the apparent (*in vivo*) K_{Dapp} of [^{18}F]nifene in the rhesus monkey (3 ± 1 pmol/mL, Hillmer et al., 2012), we approximate that the $\alpha 4\beta 2^*$ receptor occupancy due to the nifene mass present from radioligand injections is less than 5% throughout the course of both experiments. The potential effects of a small nifene mass build-up from the multiple radioligand injections on these experiments would likely be negligible due to the presence of nearly saturating doses of (–)nicotine or lobeline at the receptor site during the second and third [^{18}F]nifene injections.

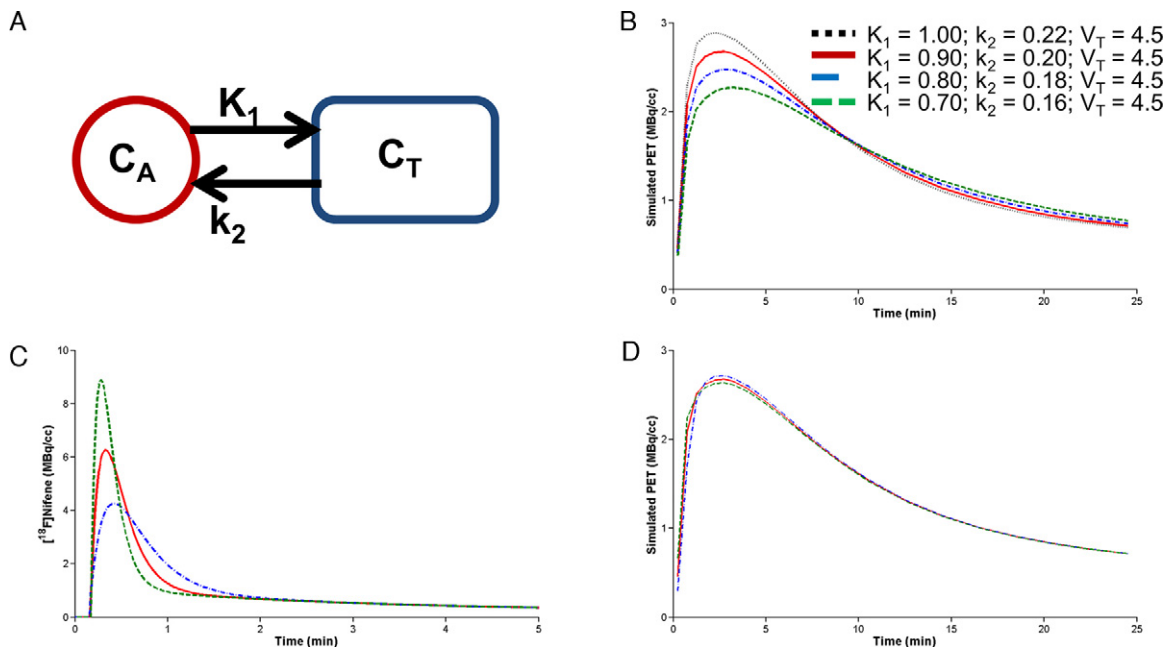


Fig. 6. Simulations of [^{18}F]nifene. (A) The one-tissue compartment model. (B) Simulated PET signal with values of K_1 and k_2 individually changed while keeping a fixed ratio of $K_1/k_2 = 4.5$. (C) Simulated input functions with different shapes but a constant area. (D) The modeled PET signal resulting from the input functions in (C).

The administration of (–)nicotine induced displacement of [¹⁸F]nifene in the cerebellum, as evidenced by the perturbation of the time–activity curves in Fig. 4. Our earlier work has shown the cerebellum to be a valid reference region for [¹⁸F]nifene in the rhesus monkey (Hillmer et al., 2011), while previous studies in rats suggested that nicotine had little effect on the time course of [¹⁸F]nifene in the cerebellum (Kant et al., 2011). The displacement of [¹⁸F]nifene in the cerebellum observed with the experiments reported herein indicate the presence of significant $\alpha 4\beta 2^*$ nAChR binding in the rat cerebellum. This finding is in agreement with studies using an analog radioligand of [¹⁸F]nifene, 2-[¹⁸F]FA-85380, which found the cerebellum to contain small amounts of specific binding in the rat brain (Vaupeul et al., 2007). Since no MRI data was acquired for partial volume correction or precise region delineation, the identified ROI may have contained spill-in signal from surrounding structures or slightly inaccurate region identification. A stereotaxic atlas was used to minimize these effects. The presence of detectable [¹⁸F]nifene binding in the cerebellum must be considered in the analysis of future experiments in the rat model to accurately quantify [¹⁸F]nifene binding.

Lobeline has pharmacological characteristics that make it preferable to other drugs as a blocking agent at the $\alpha 4\beta 2^*$ receptor. Both cytosine and nicotine exhibit broad pharmacological profiles as they bind with high affinity to a wide range of nAChR subtypes, including $\alpha 2\beta 2$, $\alpha 2\beta 4$, $\alpha 3\beta 2$, $\alpha 4\beta 2$, and $\alpha 4\beta 4$ (Parker et al., 1998). While lobeline has a similar affinity compared to cytosine and nicotine for the $\alpha 4\beta 2$ subtype, it has a much lower affinity for the other subtypes, particularly those containing the $\beta 4$ subunit (Parker et al., 1998). Lobeline has also been found to be roughly 10 times less potent at the $\alpha 7^*$ nAChR compared to nicotine and cytosine (Houlihan et al., 2001; Miller et al., 2004), giving it advantages over nicotine and cytosine in selectivity for the $\alpha 4\beta 2$ subtype. Additionally, chronic exposure of both nicotine and cytosine has been found to upregulate nAChR expression, while this effect is not observed with lobeline (Bhat et al., 1991; Riganti et al., 2005). As a result, measurement of binding levels with PET experiments in subjects with long-term cytosine or nicotine exposure would be increased relative to subjects naïve to these drugs. Lobeline may be preferable as a partial agonist in repeated nAChR-blocking PET experiments if a nicotine-naïve state is desired for these subjects.

PET imaging techniques have been used to quantify the saturation of $\alpha 4\beta 2^*$ nAChRs by cigarettes (Brody et al., 2006), however, they have not been extensively used to evaluate smoking treatment drugs. The PET experiments presented herein show rapid displacement of [¹⁸F]nifene by lobeline, demonstrating the fast-acting nature and high affinity of the drug *in vivo*. Additionally, the cerebral distribution of drug efficacy can be evaluated. Similar imaging protocols hold potential for further use in evaluating drugs such as lobeline given explicitly for smoking cessation (e.g. at therapeutic dosages and administration routes).

4.2. Effects of lobeline on [¹⁸F]nifene transport rates

The main purpose of the second experimental design was to determine if lobeline altered the delivery of [¹⁸F]nifene between the arterial plasma and the tissue. To accomplish this, (–)nicotine was first given to saturate $\alpha 4\beta 2^*$ specific binding. The PET signal from [¹⁸F]nifene could then be measured with no specific binding component. A second injection of [¹⁸F]nifene following lobeline dosing was then used to examine changes in plasma-to-tissue influx and efflux.

Initial [¹⁸F]nifene delivery following the administration of lobeline was consistently reduced compared to the control condition, as shown in Fig. 5. At later times, however, the time courses were indistinguishable. Assuming the time course of [¹⁸F]nifene in the plasma is similar for both injections, the reduction in initial

[¹⁸F]nifene uptake following lobeline administration is consistent with lobeline reducing both K_1 and k_2 within the framework of the 1TCM. Since the late cerebellar concentrations both pre- and post-lobeline were the same, it can be concluded that the distribution volumes ($V_T = K_1/k_2$) remained unchanged. The transporter of interest is a carrier-mediated process (Diamond, 1971), therefore transport is assumed to be bidirectional and both K_1 and k_2 would be expected to be altered by inhibition of this mechanism, given sufficient time to reach equilibrium.

Simulations illustrated that reducing both K_1 and k_2 by 10–15% produced changes to the corresponding PET signal similar to those observed before and after lobeline blocking. If (–)nicotine were to incompletely block binding of [¹⁸F]nifene and specific binding were present, then the k_2 parameter expands to $k'_2 = k_2/(1 + BP_{ND})$, where BP_{ND} is the binding potential specific to a reference region with nondisplaceable radioligand uptake and represents specific binding. Since lobeline is active at the $\alpha 4\beta 2^*$ nAChR site, any possible changes to specific binding would decrease BP_{ND} , resulting in an increase in k'_2 . This is inconsistent with the simulated decrease in k_2 , and suggests that the changes observed in [¹⁸F]nifene following the administration of lobeline are not due to changes in specific binding.

Possible blood flow dependent variations to the input function at early time points were examined by broadening and sharpening the shape to simulate alterations to delivery of radioligand to the tissue. The simulated PET data indicated a small change in the modeled PET signal at early time points that is also qualitatively similar to the changes observed experimentally. Deviations to the shape of the input function could be due to a number of causes, including differences in bolus delivery or alterations in blood flow. While a consistent heart rate was observed throughout the course of these experiments, this observation does not necessarily translate to a consistent blood flow, particularly at the sensitive levels pertinent to these findings. Therefore alterations to blood flow must be considered as a possible source of the observed changes in uptake rates with and without lobeline.

The physiological basis for the changes in [¹⁸F]nifene transport rates due to lobeline is unclear. A previous examination of modifications to cerebral blood flow with the radioligands [¹¹C]raclopride and [¹¹C]cocaine resulted in equivalent variations in both K_1 and k_2 values, thus maintaining the same V_T (Logan et al., 1994). Since Fig. 6B illustrates that the effects of lobeline decreased both K_1 and k_2 in equal magnitude, it is therefore possible that the variations in [¹⁸F]nifene delivery to the tissue are due to decreases in the blood flow, potentially induced by the pharmacological effects of lobeline. Alternatively, the presence of lobeline may inhibit the transport of [¹⁸F]nifene across the BBB. The reported K_T of lobeline for the BBB amine transporter is 400 μM (Allen et al., 2003). The experiments reported herein were limited to a 0.6 μmol (3 $\mu\text{mol}/\text{kg}$) lobeline dose due to the toxicity of the compound. Assuming a 10 mL blood volume for the rat, the lobeline concentration could be speculated at roughly 60 μM once the drug equilibrated between the plasma and transporter, not correcting for lobeline metabolism. Potential interactions of lobeline with the BBB amine transporter at doses less than 3 $\mu\text{mol}/\text{kg}$ are likely below the detection sensitivity of PET experiments. The BBB amine transporter possibly interacts with the class of $\alpha 4\beta 2^*$ nAChR radioligands in general, as an interaction with this transporter was previously observed in experiments with [¹⁸F]flubatine (formerly [¹⁸F]NCFHEB, (Deuther-Conrad et al., 2008)).

The BBB amine transporter is important as a candidate for understanding the mechanism underlying the physiological processes governing transfer of [¹⁸F]nifene from the plasma to the tissue. Evidence of an inverse parabolic relationship between lipophilicity and extraction across the blood–brain barrier has been well established by previous experiments (Dischino et al., 1983;

Kessler et al., 1991; Waterhouse, 2003). Our previous work reported a high [^{18}F]nifene K_1 value of 0.9 mL/min/cm 3 in the rhesus monkey (Hillmer et al., 2012), which would suggest near complete extraction of radioligand from the plasma to the tissue. However, the $-0.5 \log P$ value of [^{18}F]nifene (Pichika et al., 2006) would predict an extraction of [^{18}F]nifene into the tissue of roughly 75% due to passive diffusion (Dischino et al., 1983). A mechanism beyond simple diffusion at the BBB would help explain the high extraction of [^{18}F]nifene from plasma to tissue. Further studies with blood sampling to allow for complete modeling of [^{18}F]nifene kinetics in the presence of lobeline are required to confirm the role of a potential transporter. *In vitro* studies which control cerebral blood flow may also be necessary to isolate the influence of lobeline at the transporter from blood flow effects.

5. Conclusion

The presented experiments indicate that lobeline competes with bound [^{18}F]nifene at the $\alpha 4\beta 2^*$ nAChR site. Displacement of [^{18}F]nifene was observed not only in the receptor-rich region of the thalamus, but also in the cerebellum, indicating that the cerebellum may not be an appropriate reference region for the rat model. Evidence of reduced [^{18}F]nifene plasma-to-tissue transport and clearance in the presence of lobeline was observed, however, it could not be distinguished if this resulted from blood flow effects or inhibition of the BBB amine transporter. The effects of lobeline at the BBB amine transporter requires closer inspection to better understand this interaction and its effect on [^{18}F]nifene transport. The experimental methods presented here can be used for future PET experiments for better understanding the pharmacological mechanisms of drugs developed for the treatment of smoking addiction.

Acknowledgements

We thank Professor R. Jerry Nickles and Hector Valdovinos for assistance with isotope production. We are grateful to Professor Jim Holden and Dr. Alex Converse for technical discussions. We also thank Elaine Luong for assistance with animal housing. This work was supported by NIH grant MH086014.

References

- Albuquerque EX, Pereira EF, Alkondon M, Rogers SW. Mammalian nicotinic acetylcholine receptors: from structure to function. *Physiol Rev* 2009;89:73–120.
- Allen DD, Lockman PR, Roder KE, Dwoskin LP, Crooks PA. Active transport of high-affinity choline and nicotine analogs into the central nervous system by the blood-brain barrier choline transporter. *J Pharmacol Exp Ther* 2003;304:1268–74.
- Bhat RV, Turner SL, Selvaag SR, Marks MJ, Collins AC. Regulation of brain nicotinic receptors by chronic agonist infusion. *J Neurochem* 1991;56:1932–9.
- Brioni JD, Decker MW, Sullivan JP, Arneric SP. The pharmacology of (–)-nicotine and novel cholinergic channel modulators. *Adv Pharmacol* 1996;37:153–214.
- Brody AL, Mandelkern MA, London ED, Olmstead RE, Farahi J, Scheibal D, et al. Cigarette smoking saturates brain $\alpha 4\beta 2$ nicotinic acetylcholine receptors. *Arch Gen Psychiatry* 2006;63:907–15.
- Burghaus L, Schütz U, Krempel U, Lindstrom J, Schröder H. Loss of nicotinic acetylcholine receptor subunits $\alpha 4$ and $\alpha 7$ in the cerebral cortex of parkinson patients. *Parkinsonism Relat Disord* 2003;9:243–6.
- Christian BT, Vandehey NT, Floberg JM, Mistretta CA. Dynamic PET denoising with HYPR processing. *J Nucl Med* 2010;51:1147–54.
- Constantinescu CC, Mukherjee J. Performance evaluation of an Inveon PET preclinical scanner. *Phys Med Biol* 2009;54:2885–99.
- Court J, Martin-Ruiz C, Piggott M, Spurdin D, Griffiths M, Perry E. Nicotinic receptor abnormalities in Alzheimer's disease. *Biol Psychiatry* 2001;49:175–84.
- Damaj MI, Patrick GS, Creasy KR, Martin BR. Pharmacology of lobeline, a nicotinic receptor ligand. *J Pharmacol Exp Ther* 1997;282:410–9.
- Deuther-Conrad W, Patt JT, Lockman PR, Allen DD, Patt M, Schildan A, et al. Norchloro-fluoro-homoepibatidine (NCFHEB) – a promising radioligand for neuroimaging nicotinic acetylcholine receptors with PET. *Eur Neuropsychopharmacol* 2008;18:222–9.
- Diamond I. Choline metabolism in brain. The role of choline transport and the effects of phenobarbital. *Arch Neurol* 1971;24:333–9.
- Dischino D, Welch MJ, Kilborun MR, Raichle ME. Relationship between lipophilicity and brain extraction of C-11-labeled radiopharmaceuticals. *J Nucl Med* 1983;24:1030–8.
- Happe HK, Peters JL, Bergman DA, Murrin LC. Localization of nicotinic cholinergic receptors in rat brain: autoradiographic studies with [^3H]cytisine. *Neuroscience* 1994;62:929–44.
- Hillmer AT, Wooten DW, Moirano JM, Slesarev M, Barnhart TE, Engle JW, et al. Specific $\alpha 4\beta 2$ nicotinic acetylcholine receptor binding of [F-18]nifene in the rhesus monkey. *Synapse* 2011;65:1309–18.
- Hillmer AT, Wooten DW, Slesarev M, Ahlers EO, Barnhart TE, Murali D, et al. PET imaging of $\alpha 4\beta 2^*$ nicotinic acetylcholine receptors: quantitative analysis of ^{18}F -nifene kinetics in the nonhuman primate. *J Nucl Med* 2012;53:1471–80.
- Horti A, Scheffel U, Stathis M, Finley P, Ravert HT, London ED, et al. Fluorine-18-FPH for PET imaging of nicotinic acetylcholine receptors. *J Nucl Med* 1997;38:1260–5.
- Houlihan LM, Slater Y, Duerra DL, Peng J-H, Kuo Y-P, Lukas RJ, et al. Activity of cytosine and its brominated isosteres on recombinant human $\alpha 7$, $\alpha 4\beta 2$ and $\alpha 4\beta 4$ nicotinic acetylcholine receptors. *J Neurochem* 2001;78:1029–43.
- Kant R, Constantinescu C, Parekh P, Pandey SK, Pan M-L, Easwaramoorthy B, et al. Evaluation of ^{18}F -nifene binding to $\alpha 4\beta 2$ nicotinic receptors in the rat brain using microPET imaging. *EJNMMI Res* 2011;1:1–9.
- Kassiou M, Scheffel UA, Ravert HT, Mathews WB, Musachio JL, London ED, et al. Pharmacological evaluation of [^{11}C]A-84543: an enantioselective ligand for *in vivo* studies of neuronal nicotinic acetylcholine receptors. *Pharmacol Lett* 1998;63:13–8.
- Kessler RM, Ansari MS, de Paulis T, Schmidt DE, Clanton JA, Smith HE, et al. High affinity dopamine D2 receptor radioligands. 1. Regional rat brain distribution of iodinated benzamides. *J Nucl Med* 1991;32:1593–600.
- Logan J, Volkow ND, Fowler JS, Wang G-J, Dewey SL, MacGregor R, et al. Effects of blood flow on [^{11}C]raclopride binding in the brain: model simulations and kinetic analysis of PET data. *J Cereb Blood Flow Metab* 1994;14:995–1010.
- Miller DK, Crooks PA, Zheng G, Grinevich VP, Norrholm SD, Dwoskin LP. Lobeline analogs with enhanced affinity and selectivity for plasmalemma and vesicular monoamine transporters. *J Pharmacol Exp Ther* 2004;310:1035–45.
- Miller DK, Lever JR, Rodvelt KR, Baskett JA, Will MJ, Lobeline KGR. A potential pharmacotherapy for drug addiction, binds to (–)-opioid receptors and diminishes the effects of opioid receptor agonists. *Drug Alcohol Depend* 2007;89:282–91.
- Muzic RF, Cornelius S. COMKAT: compartment model kinetic analysis tool. *J Nucl Med* 2001;42:636–45.
- Parker MJ, Beck AV, Luetje CW. Neuronal nicotinic receptor $\beta 2$ and $\beta 4$ subunits confer large differences in agonist binding affinity. *Mol Pharm* 1998;54:1132–9.
- Paxinos G, Watson C. The rat brain in stereotaxic coordinates. 4th ed. San Diego: Academic Press; 1998.
- Pichika R, Easwaramoorthy B, Collins D, Christian BT, Shi B, Narayanan TK, et al. $\alpha 4\beta 2$ receptor imaging agents: part II. Synthesis and biological evaluation of 2-[^{18}F]fluoro-3-[2-((S)-3-pyrrolinyl)methoxy]pyridine (^{18}F -nifene) in rodents and imaging by PET in nonhuman primate. *Nucl Med Biol* 2006;33:295–304.
- Poirier M-F, Canceil O, Baylé F, Millet B, Bourdel M-C, Moatti C, et al. Prevalence of smoking in psychiatric patients. *Prog Neuropsychopharmacol* 2002;26:529–37.
- Riganti L, Matteoni C, Di Angelantonio S, Mistri A, Gaimarri A, Sparatore F, et al. Long-term exposure to the new nicotinic antagonist 1,2-bisN-cytisinylethane upregulates nicotinic receptor subtypes of SH-SY5Y human neuroblastoma cells. *Br J Pharmacol* 2005;146:1096–109.
- Teng L, Crooks PA, Sonsalla PK, Dwoskin LP. Lobeline and nicotine evoke [^3H]overflow from rat striatal slices preloaded with [^3H]dopamine: differential inhibition of synaptosomal and vesicular [^3H]dopamine uptake. *J Pharmacol Exp Ther* 1997;280:1432–44.
- Vaupel DB, Stein EA, Mukhin AG. Quantification of $\alpha 4\beta 2^*$ nicotinic receptors in the rat brain with microPET and 2-[^{18}F]F-A-85380. *NeuroImage* 2007;34:1352–62.
- Waterhouse RN. Determination of lipophilicity and its use as a predictor of blood-brain barrier penetration of molecular imaging agents. *Mol Imaging Biol* 2003;5:376–89.